Estimating the Ground-Motion Distribution of the 2016 M_w 6.2 Amatrice, Italy, Earthquake Using Remote Infrasound Observations

by Bruno Hernandez, Alexis Le Pichon, Julien Vergoz, Pascal Herry, Lars Ceranna, Christoph Pilger, Emanuele Marchetti, Maurizio Ripepe, and Rémy Bossu

ABSTRACT

The M_w 6.2 Amatrice earthquake that struck central Italy on 24 August 2016 was recorded by seven infrasound arrays in the Euro-Mediterranean region at distances up to 1260 km. Most stations recorded long-lasting coherent wavetrains characterized by large back-azimuth variations. The backprojection of the stratospherically ducted infrasound recorded at five arrays illuminates radiating regions over ~600 km along the Apennines from the Po basin to the Gulf of Naples. A comparison between the acoustic surface pressure derived from infrasound records and the seismic source pressure derived from measured seismic ground motion shows first-order agreement in the attenuation with the epicentral distance. From these observations, seismic quality factors in central Italy are estimated. The northernmost reconstructed source region comprises the Po Valley where seismic amplification occurred within the plain alluvial sediments. These results show that infrasound records at hundreds of kilometers from a shallow moderate magnitude devastating earthquake can provide ground shaking information as well as local amplification caused by topographic and geological features.

INTRODUCTION

There are several mechanisms of low-frequency pressure wave generation in the atmosphere during earthquakes (Donn and Posmentier, 1964). Infrasound from earthquake can be generated in the epicentral area due to the sudden ground motion above the seismic source (e.g., Olson *et al.*, 2003; Madshus *et al.*, 2005). Efficient seismic to infrasound coupling often occurs with large earthquakes (local seismic magnitude $M_w > 6$) close-to-high mountain ranges (Mikumo, 1968; Le Pichon *et al.*, 2003; Mutschlecner and Whitaker, 2005; Le Pichon *et al.*, 2006; Walker *et al.*, 2013). These studies investigated the effects of both seismic source directivity and topographic features on acoustic radiation. They demonstrated that infrasound detected out to a range of ~5500 km illuminated land areas that experienced shaking, up to ranges of ~700 km from the epicentral region.

Moderately sized ($3 < M_w < 6$) shallow seismic earthquakes can also radiate pressure waves if topographic conditions are favorable. In particular, the shaking of small prominent topographic points such as coastal cliffs in the vicinity of the epicenter may act as infrasound sources (Green *et al.*, 2009). In that study, they successfully modeled the seismic to acoustic coupling along cliffs of 75 m average height by the radiation, a series of independent pistons generating acoustic waves with largest amplitudes observed along the cliff normal.

Infrasound signals from earthquakes of magnitude smaller than six allowed a better understanding of ground-to-air coupling mechanisms (Arrowsmith *et al.*, 2010). Using a 3D finite-difference method and the seismic moment tensor, Arrowsmith *et al.* (2012) modeled the acceleration in the epicentral region. The accelerations were integrated over the epicenter region using the Rayleigh integral, which was numerically solved to propagate pressure waves in the far field.

Evanescently coupled low-frequency sound from large underwater earthquake has also been observed. Evers *et al.* (2014) reported infrasound signals at 1300 km from the M_w 8.1 Macquarie Ridge earthquake. This analysis confirmed that underwater sources can produce low-frequency acoustic waves in the atmosphere from evanescent wave coupling at the water–air interface (Godin, 2008). Such studies show the capability of the infrasonic component of the International Monitoring System (IMS) deployed for the verification regime of the Comprehensive Nuclear-Test Ban Treaty (CTBT; Marty, 2018) to detect and characterize underground explosions (Assink *et al.*, 2016).

The 24 August 2016 M_w 6.2 Amatrice earthquake (42.71° N and 13.22° E, at a shallow depth of 4 km, about 45 km north of L'Aquila, central Italy) occurred on a northwest–southeast normal fault segment striking along the Apennines (Chiaraluce *et al.*, 2017). It was followed by an M_w 5.5 (02:33 UTC) aftershock located about 10 km northeast of the mainshock (Michele *et al.*, 2016). This region has experienced

doi: 10.1785/0220180103

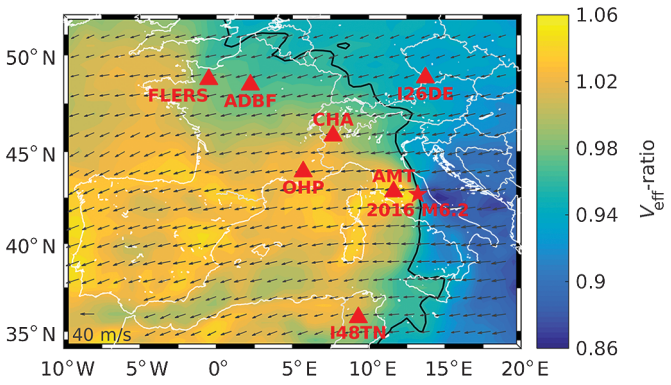

▲ **Figure 1.** Geographical map showing the arrays (red triangles) that recorded infrasound from the M_w 6.2 Amatrice earthquake. The epicenter is indicated by the red star. Background colors indicate the ratio of the maximum effective sound speed (static sound speed plus along-path wind speed) between 30 and 60 km to the sound speed at the ground level. The black solid line corresponds to $V_{eff-ratio} = 1$. All stations, except I26DE, are located downwind ($V_{eff-ratio} > 1$) in regions where stratospheric returns are expected. The temperature and wind vertical profiles over the studied regions are extracted from the European Centre for Medium-Range Weather Forecasts (ECMWF) operational analyses part of the Integrated Forecast System (IFS) cycle 38r2, introducing a higher vertical resolution of 137 levels with a model top at 0.01 hPa (~78 km). The arrows indicate the wind fields at 50 km altitude.

a number of significant earthquakes in recent history. The series of earthquake that occurred in 1997 in the regions of Umbria and Marche included events of magnitude larger than 5.0 in a two-month period (Amato *et al.*, 1998; Hernandez *et al.*, 2004). The M_w 6.3 earthquake that occurred on 6 April 2009 followed by a strong aftershock sequence caused serious damage in the city of l'Aquila and surroundings (Chiarabba *et al.*, 2009).

This event was recorded by multiple infrasound stations in the Euro-Mediterranean region. The analysis of the recorded signals in different directions offers an opportunity to better understand the source mechanism of pressure wave generation involved in moderately sized earthquakes. Shani-Kadmiel *et al.* (2018) analyzed infrasonic signals detected at one IMS station (I26DE) from the M_w 6.2 Amatrice earthquake. In addition to the epicentral infrasound, they identified patches of diffracted signals in the Po Valley and in the Austrian Alps. In this study, we analyze infrasonic waves detected hundreds of kilometers away from the epicenter by two arrays that are part of IMS (I26DE, Germany; I48TN, Tunisia) and five experimental arrays (AMT, Italy; CHA, Italy; FLERS, France; ADBF, France; and OHP, France). These multiple station infrasonic observations combined with ground shaking measured by the dense Italian seismic network are valuable to recover a comprehensive image of the acoustic source regions associated with seismic-to-acoustic wave conversion.

Detailed analyses of the signals recorded at all operating arrays are first presented. The epicentral source region is inverted by applying a grid-search location procedure. By combining infrasound measurements at several arrays, ground-truth information and detailed propagation models, epicentral and diffracted source regions are reconstructed and compared with ground motion measured by the National Seismic Network operated by Istituto Nazionale di Geofisica e Vulcanologia (INGV), and the national accelerometric network (RAN) operated by the Italian Civil Protection Department (Luzi *et al.*, 2016, 2017).

These results highlight the potential of infrasonic arrays to remotely locate and measure the amplitude of surface shaking during moderate earthquakes. During the 2012 M_w 5.9 Ferrara earthquake that struck northern Italy (Piccinini *et al.*, 2012), the location and extent of the infrasound radiant area matched the peak ground acceleration (PGA) map, providing the link between the acoustic source and seismic amplification within the Po plain alluvial sediments (Marchetti *et al.*, 2016). Our results provide additional evidence to support the potential value of infrasound to generate ShakeMaps in which accelerometer networks are not well developed. ShakeMaps provide near-real-time maps of ground motion and shaking intensity following significant earthquakes. These maps are used by federal, state, and local organizations, both public and private, for postearthquake response and recovery, public, and scientific information, as well as for preparedness exercises and disaster planning.

INFRASOUND MEASUREMENTS

Even though the infrasound network of the IMS is not fully established, it already provides a uniform coverage for locating man-made and natural sources worldwide (Mialle *et al.*, 2018). In addition, national seismoacoustic monitoring systems have been developed in central Europe over several decades filling a gap in the global IMS network. The detection and location capability of the combined network is significantly enhanced offering a unique opportunity to investigate improved methods for discriminating between natural and artificial acoustic sources (e.g., Gibbons *et al.*, 2015), and better understand seismoacoustic coupling mechanism at the earth-atmosphere interface.

Figure 1 shows the 2D field of the effective sound speed ratio ($V_{eff-ratio}$) in the stratosphere (30–60 km altitude) over the region of interest. In the high-frequency approximation, values of $V_{eff-ratio}$ above one indicate favorable downwind propagation in the stratospheric duct. At the time of the event, easterly stratospheric wind flow favored an efficient ducting through the stratospheric waveguide toward stations located west of the seismic source.

Figure 2 shows the filtered infrasound records of the mainshock and M_w 5.5 aftershock. At AMT, the dominant frequency is about 0.4 Hz at a maximum signal amplitude of ~5 Pa peak-to-peak. Clear signals are observed at AMT, CHA, OHP, and I26DE. Signals are detected as far as FLERS (1258 km) for the mainshock, and OHP (623 km) for the M_w 5.5 aftershock. The effect of the stratospheric winds on the attenuation is clearly visible when comparing signal amplitude at I26DE (upwind) and OHP (downwind) which are

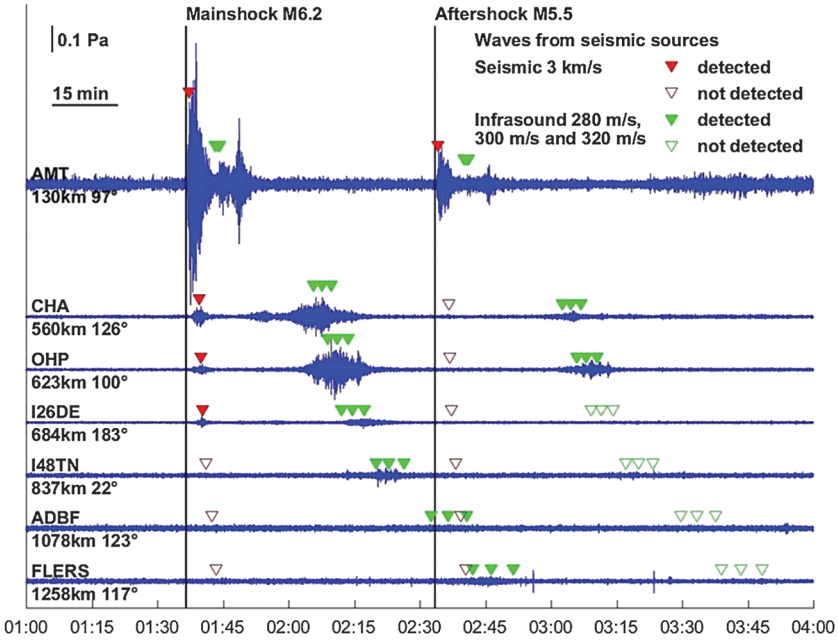

▲ **Figure 2.** Infrasound time series recorded at seven arrays sorted by distance. Only one array element was available at AMT. Waveforms are filtered in the 0.2–0.8 Hz band. Red and green triangles indicate the theoretical arrival times for typical celerity values of seismic surface waves (3 km/s) and stratospheric arrivals (280, 300, and 320 m/s). Detections of seismic and infrasound waves are indicated by filled triangles.

located at about a same distance from the source (Table 1). Given the origin of the mainshock and aftershock, infrasound signals travel with celerity range values typical of stratospheric propagation (Brown *et al.*, 2002). The celerity at the maximum signal amplitude at all arrays is close to 0.3 km/s.

The wave parameters of the signals are calculated using the progressive multi-channel correlation method (PMCC; Cansi, 1995). The recordings are filtered in different frequency bands and overlapping time windows. To process a broad frequency range of interest, 15 frequency bands logarithmically spaced between 0.05 and 4 Hz, and window lengths varying linearly with the period are used (Brachet *et al.*, 2010; Matoza *et al.*, 2013). At a sampling rate of 20 Hz, the resolution of perfectly correlated planar wavefront is about 1 m/s for the azimuth and 5 m/s for the horizontal trace velocity (Szuberla and Olson, 2004).

Figure 3 shows an example of PMCC processing results at OHP, located in the southeastern part of France at a distance of 623 km from the epicenter. Clear detections associated with the mainshock and M_w 5.5 aftershock are detected. The fastest arrival (group A) coincides with the theoretical arrival time of the seismic surface waves. This arrival is primarily the manifestation of the seismic response of the MB2005 microbarometer (Ponceau and Bosca, 2010). OHP array recorded remarkably well-defined back-azimuth variations that span the Apennines with trace velocity ranging between 0.34 and 0.38 km/s. The back azimuths of group B increase from 70° to 125°. The large azimuthal variations suggest the existence spatially extended sources of infrasound. The period of the signals peaks at 2.5 s.

LOCALIZATION OF INFRASOUND SOURCE REGION

PROPAGATION MODELING

One dominant factor controlling the capability of an infrasound network is the time varying stratospheric winds along the propagation paths (Garcés *et al.*, 1998; Drob *et al.*, 2003; Green and Bowers, 2010; Le Pichon *et al.*, 2012). At the time of the Amatrice earthquake, due to the westward stratospheric wind jet blowing at moderate speed (~50 m/s, Fig. 1), infrasound essentially propagated in the stratospheric waveguide as confirmed by the observed range of celerity values (Fig. 2). Of specific interest is the stratospheric propagation toward I26DE for $V_{\text{eff-ratio}}$ lower than one (0.96, see Table 1). At about the same distance, the signal amplitude at OHP is about four times larger. These arrivals are explained by diffraction and scattering effects which propagate energy into geometrical shadow zones, more specifically when the used atmospheric model does not resolve wind fluctuations induced by naturally occurring gravity waves or underestimate the mean along-path stratospheric winds (e.g., Green *et al.*, 2011; Le Pichon *et al.*, 2015).

Table 1
Values of the Four Parameters Following Le Pichon *et al.* (2012) Used to Compute the Attenuation for a Source Frequency of 0.4 Hz

Station	$V_{\text{eff-ratio}}$	α(km^{-1})	β	δ (km)	σ (km)
CHA	1.04	−0.39	−0.9	180	43
OHP	1.06	−0.39	−0.9	180	43
FLERS	0.98	−0.39	−1.15	180	43
I26DE	0.96	−0.39	−1.15	180	43
I48TU	0.96	−0.39	−1.15	180	43

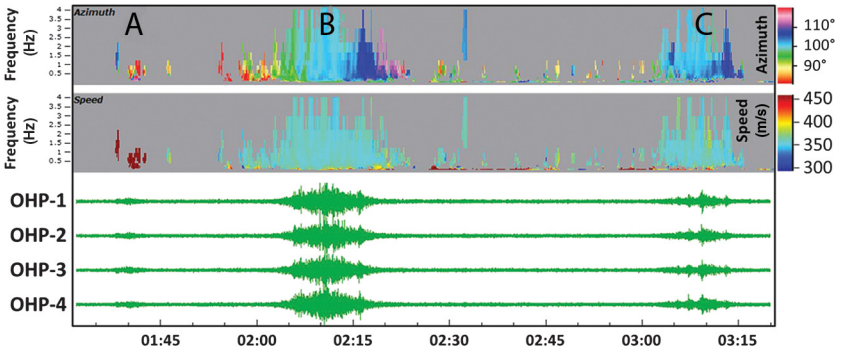

▲ **Figure 3.** Progressive multi-channel correlation method (PMCC) analysis at OHP station (UTC time). (Top) Color coded azimuth (in degree, clockwise from north) and the trace velocity (in km/s) in time–frequency diagrams. (Bottom) Pressure recordings at four elements band-pass filtered between 0.2 and 4 Hz. In the first part of the processed time sequence, signals characterized by high-trace velocity values (greater than 3 km/s) are related to local seismically coupled air waves (group A). This wave is followed by two long-lasting coherent wavetrains associated with the propagation of epicentral and diffracted waves from the mainshock and M_w 5.5 aftershock (groups B and C).

EPICENTRAL INFRASOUND

Today, the state-of-the-art atmospheric specifications and numerical modeling techniques provide a basis for propagation predictions (e.g., Waxler and Assink, 2018). The long-range infrasound propagation is here simulated using the windy atmospheric sonic propagation ray theory-based method (WASP-3D) which accounts for the longitudinal variation of the atmospheric model along the propagation paths (Virieux *et al.*, 2004; Lalande *et al.*, 2012). The ray canonical variables (slowness vector, position, and propagation time) are numerically solved by linearized hydrodynamic equations in spherical coordinates.

To quantitatively determine the optimum source location, a grid-search approach for a single-source model developed by Walker *et al.* (2013) is implemented. The optimum location is estimated by calculating the normalized sum of squares of the misfit between the observed (uncorrected measures and wind corrected) and the true back azimuths at all arrays (sum of the square of errors [SSE]):

$$\mathrm{SSE}(x,y) = \frac{1}{m}\sum_{i}^{m}\left(\frac{1}{n_i}\sum_{j}^{n_i}\left(\frac{\theta_{ij}-\theta_i^p(x,y)}{\sigma_{ij}}\right)^2\right), \quad (1)$$

in which θ_{ij} are the observed back azimuths at each array, $\sigma_{ij} = 1°$ are the associated error bars (assumed to be identical for all arrays of kilometric aperture, Szuberla and Olson, 2004), θ_i^p are the true back azimuths, i and j refer to the arrays, m, n_i refers to the number of detections at array i, and (x, y) describes the 2D horizontal spatial grid.

Following a shooting procedure, the azimuthal deviations of eigenrays sought between the source grid (5 × 5 km) covering the studied region and each array are calculated using WASP-3D. The optimum source location using the calculated back azimuths at the maximum signal amplitude is found at ~50 km from the epicenter (Fig. 4a) where the largest ground accelerations were observed by strong ground motion stations (Cirella and Piatanesi, 2016; Lanzano *et al.*, 2016). By applying wind corrections to the observed back azimuths (−1.7° for OHP, −1.5° for I26DE, and 0.5° for I48TN), the source is relocated 43 km northeast in the earthquake epicentral region (Fig. 4b). The inverted radiation zone with SSE smaller than 1 covers a circular area close to 10, 000 km^2, centered at the earthquake epicenter.

DIFFRACTED INFRASOUND

With the knowledge of the earthquake epicenter and origin time, infrasound observations at one single array can be used to reconstruct the spatial extent of area diffracting infrasound when seismic waves propagated through mountainous regions (Walker *et al.*, 2013). To recover a comprehensive image of the acoustic source regions, records with the highest signal-to-noise ratio are considered (Fig. 2). Arrays CHA, OHP, I26DE, I48TN, and FLERS provide here an excellent basis for this reconstruction. The input parameters of the location procedure include the azimuths and arrival times measured independently by each array, the origin time and coordinates of the epicenter and group velocity models for both seismic and infrasound waves in the direction of each station. In this study, we compare the spatial source distribution of the acoustic peak surface inferred from infrasound observations to the measured ground motion.

The seismic waves trapped by superficial crustal layers propagated away from the epicenter shaking the Apennines and radiating infrasound waves. The arrival time t_d of the signals is given by

$$t_d = t_0 + r/V_S + d/V_i, \quad (2)$$

in which t_0 is the earthquake origin time, r is the propagation range of seismic surface waves traveling at velocity V_S from the epicenter to the acoustic source, and d is the propagation range from the acoustic source to OHP of stratospherical arrivals celerity V_i. In this study, V_i is derived from WASP-3D simulations and V_S is set to 3.0 km/s. The crust is mainly composed of rocks with an average velocity around 3 km/s. At regional distances, the velocity of surface waves (V_S) which dominate seismic signals is about 3 km/s. A parametric analysis shows that the uncertainty on the seismic wave velocity is not crucial to improve location as it is much larger than V_i.

To reconstruct the source region of signals recorded at OHP, equation (2) is solved along discretized great circle paths given by the wind-corrected back azimuths. By applying a grid search with a grid resolution of 1 km, the source location is given by the minimum between the predicted and observed delay times source. To account for uncertainties due to the array geometry (Szuberla and Olson, 2004) and propagation

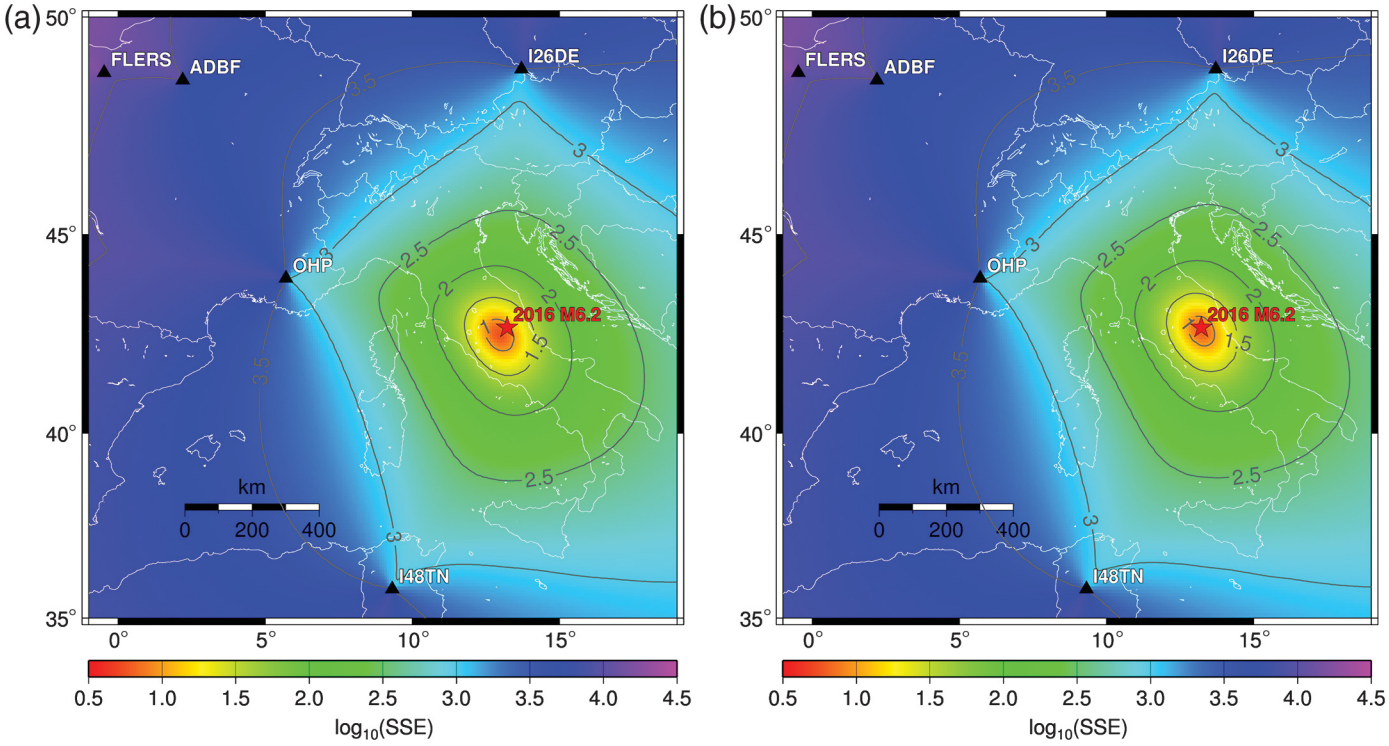

▲ **Figure 4.** Source location of epicentral infrasound generated by the 24 August 2016 M_w 6.2 Amatrice earthquake constrained by detections at stations I26DE, I48TN, and OHP arrays. The colorbar codes the misfit function sum of the square of errors (SSE) of the grid search minimizing the difference between the predicted and observed back azimuths (equation 1). Black curves are isocontours of $\log_{10}$(SSE). Location results are shown using the (a) detected and (b) wind-corrected back azimuths using windy atmospheric sonic propagation ray theory-based method (WASP-3D). (a) The location result obtained using uncorrected back azimuths (without wind correction). (b) Wind correction.

effects (e.g., Antier *et al.*, 2007; Assink *et al.*, 2014), a range of uncertainty of ±1° for the wind-corrected back azimuths and ±10 m/s for the celerity are incorporated in the location procedure. At a range of 500 km from the array, these uncertainties yield lateral and longitudinal errors in the source location of 20 and 40 km, respectively.

The detection capability of the monitoring network can be assessed by predicting the pressure wave attenuation at the receivers from the known source location. By using a frequency-dependent semiempirical attenuation relationship (equation 2 in Le Pichon *et al.*, 2012), the attenuation of the recorded signals from a reference distance to the source can be estimated (Walker *et al.*, 2013). This relation describes the attenuation by accounting for the dominant signal frequency of 0.4 Hz, the along-path stratospheric effective sound speed derived from European Centre for Medium-Range Weather Forecasts (ECMWF) Integrated Forecast System (IFS) operational analyses, geometrical spreading and dissipation of both stratospheric and thermospheric waves. Table 1 summarizes values of the four parameters α, β, δ, and σ of the attenuation relation used to compute the backprojected sound pressure level (SPL, standard reference pressure of 20 μPa) from the measured peak-to-peak pressure at the infrasound arrays.

Figure 5 compares the spatial distribution of backprojected and wind-corrected infrasound as recorded at the five nearest arrays. Measurements at OHP illuminate a continuous coupling region along the Apennine range from the Po basin in the Ligurian Apennines to the Mount Vesuvius in the Gulf of Naples. From I48TN and FLERS, infrasound sources coincide with the spatial distribution of strong ground motion in the epicenter area (Lanzano *et al.*, 2016). In addition to the epicentral zone, I26DE illuminates the northernmost coupling region in the plain of the Po River.

FROM SURFACE PRESSURE TO GROUND MOTION

Strong ground motion records released by the Italian accelerometric network (RAN) and the Italian seismic network (RSN) were considered within 48 hrs following the mainshock to compute a kinematic model of the coseismic rupture (Luzi *et al.*, 2016). During the Amatrice earthquake, the amplitude of ground shaking exhibited significant variability in the direction of the Apennines as a result of shallow normal faulting along the strike of geologically active faults. This event resulted in a bilateral along-strike rupture with a predominant rupture directivity toward north–northwest explained by a pronounced slip distribution (Tinti *et al.*, 2016).

In the present study, 122 vertical accelerograms from RAN and INGV stations located at an epicentral distance lower than 200 km are used (see Data and Resources). This near-field seismological dataset are completed with 265 unsaturated broad-

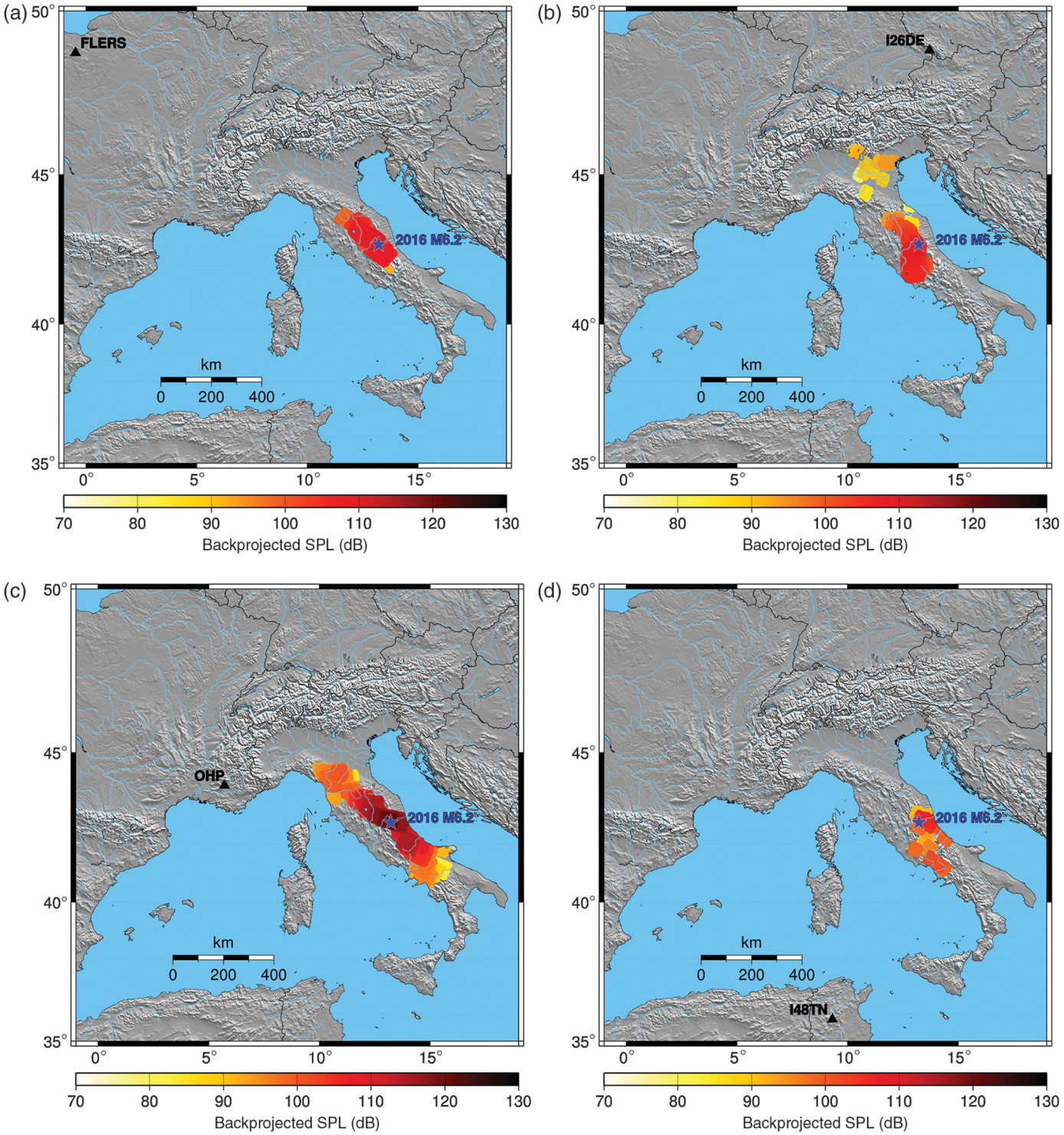

▲ **Figure 5.** Backprojected infrasound from the M_w 6.2 Amatrice earthquake corrected for geometrical spreading and dissipation with respect to a reference distance of 5 km to the earth's surface. The colorbar codes sound pressure level values (SPL, in dB). Source regions are reconstructed using measurements at (a) FLERS, (b) I26DE, (c) OHP, and (d) I48TN.

band seismic records from INGV and the French Réseau Sismologique et géodésique Français-Réseau Large Bande Permanent (RESIF-RLBP) network (see Data and Resources; RESIF, 1995). From these records, the spatial distribution of peak surface acceleration in the Italian peninsula and southeast France is reconstructed. For comparison with infrasound measurements, seismic records are band-pass filtered between 0.2 and 0.8 Hz.

To predict the peak surface pressure (PSP) at a reference distance R_{ref}, the spatial distribution of the measured peak surface acceleration region is discretized into a grid of adjacent

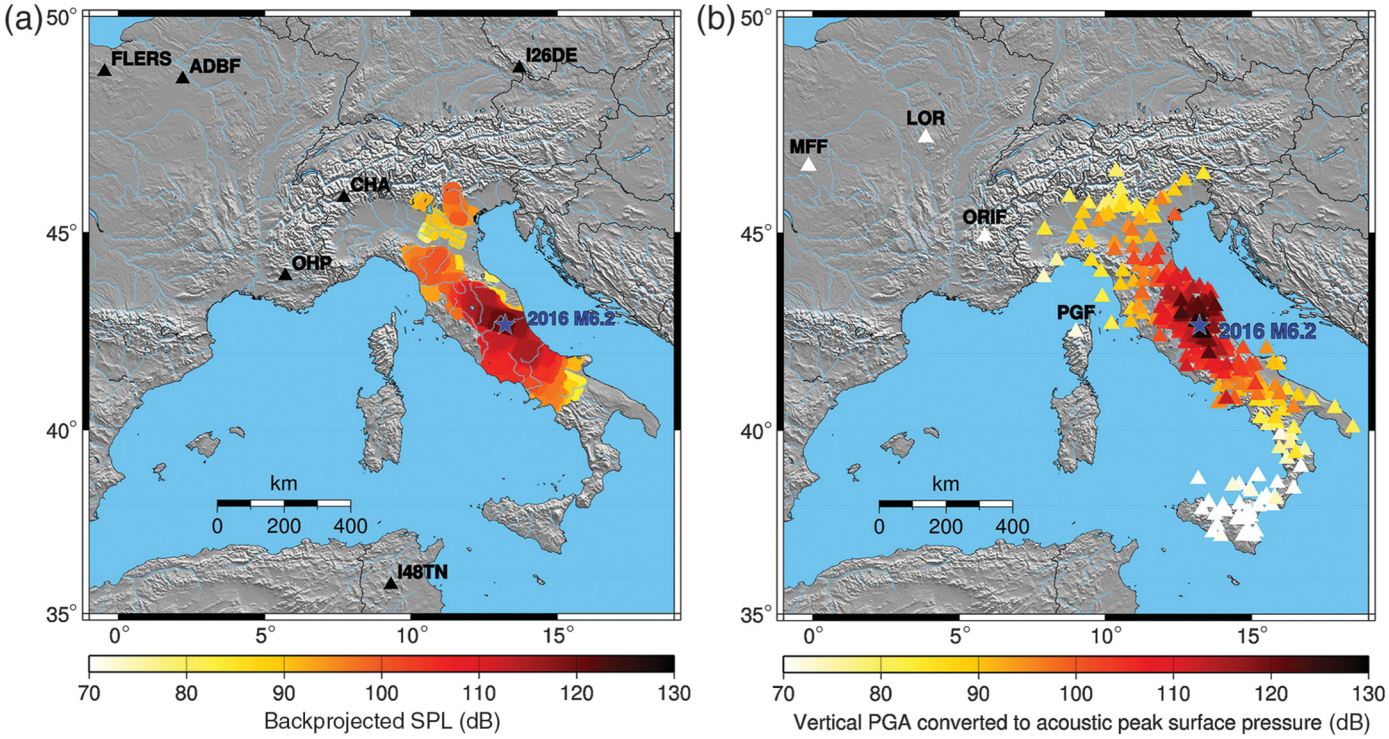

▲ **Figure 6.** Comparison between the reconstructed and measured acoustic surface pressure. (a) Backprojected infrasound (SPL, in dB) using stations CHA, FLERS, I26DE, OHP and I48TN. (b) Acoustic peak surface pressure (PSP, in dB); each triangle represents a seismic station. SPL and PSP are calculated at a reference distance R_{ref} of 5 km. (b) Peak ground acceleration (PGA) records are bandpass filtered between 0.2 and 0.8 Hz.

source elements of radius R_0 (Arrowsmith *et al.*, 2010, 2012). At the dominant frequency of the infrasound signals (0.4 Hz), the wavelength of the Rayleigh waves is about 7 km. Isophase vibration of each source element can thus be considered if R_0 remains smaller than 1 km. In the far field, when the observation distance R_{ref} (set to 5 km) is significantly larger than R_0. Under these assumptions, because the product between the acoustic wavenumber and the dimension of the radiating element is larger than one, the Rayleigh integral formulation can be used to compute PSP at a distance R_{ref} (Walker *et al.*, 2013). The spatially extended source distribution is then modeled by circular baffled pistons of radius R_0 radiating energy proportional to the surface motion normal to each vibrating element.

Figure 6 compares the cumulative view of the backprojected infrasound (SPL) to the PGA converted into PSP at the same reference distance using stations CHA, FLERS, I26DE, OHP, and I48TN. One can observe a quasi-symmetry in the north-northwest–south-southeast direction on both PSP and SPL. This symmetry reflects a bilateral source directivity consistent with the effects of the rupture directivity on ground shaking as the mainshock ruptured a north-northwest–south-southeast striking (Tinti *et al.*, 2016).

DISCUSSION AND CONCLUDING REMARKS

The M_w 6.2 Amatrice earthquake generated infrasonic waves that were observed up to a range of 1300 km by multiple stations in the Euro-Mediterranean region. 3D raytracing simulations predict a dominant stratospheric propagation for all stations. An extended radiating zone is recovered near the epicenter where the largest ground motions were measured. The observed azimuthal variations of the recorded infrasound signals are explained with the increase of effective source regions when the seismic surface waves traveled through the Apennines and reradiation occurred. The acoustic radiation by the topography can be modeled by the superposition of independent isophase baffled sources modeled using the Rayleigh integral.

Infrasound records illuminate well with the complex geometry of land areas that experienced shaking. Even the spatial extent of the radiating zones differs from one station to another as the results of source and propagation effects; it is noteworthy that consistent amplitudes of ground shaking can be inferred from pressure waves recorded at hundreds of kilometers from the epicenter.

When combining observations at multiple stations, the infrasound source regions extend over ~600 km along the Apennines from the Po basin to the Gulf of Naples. The backprojection of the stratospherically ducted infrasound observed at CHA, OHP, I26DE, I48DE, and FLERS recovers large-scale features of surface shaking where significant ground motion was measured. Figure 7 presents the cumulative view of SPL and PSP versus the epicentral distance in the northwest and southeast direction. In the 0.2–0.8 Hz band, a first-order agreement is noted in the acoustic and seismic source pressure decay

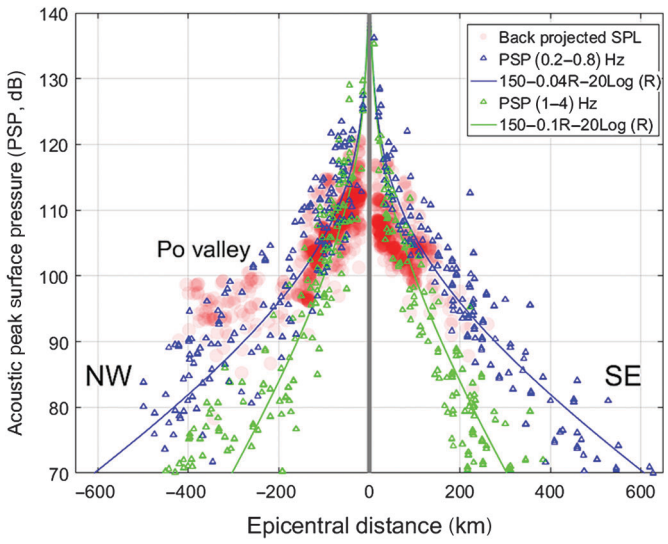

▲ **Figure 7.** Comparison between the backprojected SPL (in red) derived from infrasound records at CHA, OHP, I26DE, I48DE, and FLERS and the acoustic PSP derived from the measured seismic ground motion (PGA). PSP is plotted against the epicentral distance in the northwest and southwest direction. Seismic data are band-pass filtered between 0.2–0.8 Hz (blue triangles) and 1–4 Hz (green triangles). Solid lines are the curve fitting of PSP measurements (blue and green curves for the 0.2–0.8 Hz and 1–4 Hz frequency band, respectively).

with distance in both directions. From the epicentral region, SPL decreases by about 30 dB up to 200 km. In the northwest direction, infrasound from CHA and I26DE illuminates the northernmost source region up to distances of 400 km from the epicenter. From 200 to 400 km, SPL is roughly constant ranging between 90 and 100 dB. This region comprises the Po Valley where no significant acoustic radiation contributions from nearby mountain ranges are expected. Such observation is consistent with seismic amplification induced by earthquake interaction within the Po plain alluvial sediments (Marchetti *et al.*, 2016) which is highlighted in the northwest–southeast asymmetry of SPL and PSP attenuation. At higher frequencies (1–4 Hz), PSP decreases more rapidly with distance with a quasi-symmetry in the northwest–southeast direction.

In Figure 7, the PSP attenuation is fitted with the analytical attenuation equation

$$A_0 - \alpha R - 20\log_{10}(R)(\text{in dB}), \tag{3}$$

in which A_0 is the amplitude at the epicenter (here set to 150 dB) and R is the epicentral distance. The $-20\log_{10}(R)$ term corresponds to the body-wave geometric expansion. The $-\alpha R$ term represents the inelastic absorption and attenuation of the maximum amplitude due to scattering effects. From this curve fitting, we obtain a quality factor $Q_{0.4\text{ Hz}} = 65 \pm 20$ for $\alpha = 0.04$ and $Q_{2\text{ Hz}} = 125 \pm 30$ for $\alpha = 0.1$. These values are consistent with seismic quality factors estimated in central Italy by Pisconti *et al.* (2015).

For this specific event, it is shown that without seismic data, infrasound records only can provide information on the variation of the seismic amplitude with the epicentral distance.

Seismicacoustic coupling involves ground-to-air wave conversion associated to the propagation of seismic waves, wave diffraction in heterogeneous medium and long-range infrasound propagation in realistic atmosphere. A rigorous modeling of the ground acceleration effect on seismoacoustic coupling would require a detailed representation of the topography and associated radiation patterns to be considered. In particular, as surface-wave scattering is significant for propagation through pronounced topography, the amplitude and phase information of individual source contributions are especially important to predict. More detailed analyses require corrections for the effects of the seismic source parameterization and topographic features (Snieder, 1986). With the increasing capability of high performance computing architectures, new numerical formulations of spectral element methods for solving elasticacoustic wave propagation in heterogeneous geological configurations open doors to model geophysical media involving complex interfaces geometries (e.g., Virieux *et al.* 2012; Terrana *et al.*, 2017).

It is expected that infrasonic observations by multiple stations will increase with the number of infrasound stations being deployed worldwide. In the absence of well-developed surface motion instrumentation, these results lead to the determination of surface shaking intensities in the epicentral region. Under favorable propagation condition, infrasound could be used as a method to evaluate the severity of shaking in a remote region faster than other methods such as onsite ground surveys. Analyzing such events is furthermore pertinent in the context of the future verification regime of the CTBT when considering infrasound from shallow underground explosions which can generate seismic disturbances of similar size (e.g., Douglas and Marshall, 1996).

DATA AND RESOURCES

ShakeMap was obtained from the ground-motion accelerometric database from the Italian Accelerometric Archive (ITACA) of the national accelerometric network (RAN, http://ran.protezionecivile.it/, last accessed August 2018) operated by the Italian Civil Protection Department—Presidency of the Council of Ministers (DPC), the National Seismic Network operated by Istituto Nazionale di Geofisica e Vulcanologia (INGV, http://esm.mi.ingv.it, last accessed August 2018), and broadband waveforms of the Réseau Sismologique et géodésique Français (RESIF) seismic data portal (http://seismology.resif.fr/, last accessed August 2018). Infrasound data are available upon request. Some plots were made using the Generic mapping Tools (www.soest.hawaii.edu/gmt, last accessed July 2017).

ACKNOWLEDGMENTS

The authors are grateful to the Comprehensive Nuclear-Test Ban Treaty Organization (CTBTO) and International

Monitoring System (IMS) station operators for guaranteeing the high-quality infrasound data. This work was performed during the course of the Atmospheric dynamics Research Infrastructure in Europe (ARISE) design study (http://arise-project.eu, last accessed August 2018) funded by the European Union's Horizon 2020 research and innovation programme under Grant Agreement Number 653980.

REFERENCES

Amato, A., R. Azzara, C. Chiarabba, G. B. Cimini, M. Cocco, M. Di Bona, L. Margheriti, S. Mazza, F. Mele, G. Selvaggi, *et al.* (1998). The 1997 Umbria-Marche, Italy, earthquake sequence: A first look at the main shocks and aftershocks, *Geophys. Res. Lett.* doi: 10.1029/98GL51842.

Antier, K., A. Le Pichon, S. Vergniolle, C. Zielinski, and M. Lardy (2007). Multiyear validation of the NRL-G2S wind fields using infrasound from Yasur, *J. Geophys. Res.* **112,** D23110, doi: 10.1029/2007JD008462.

Arrowsmith, S. J., R. Burlacu, K. Pankow, B. Stump, R. Stead, R. Whitaker, and C. Hayward (2012). A seismoacoustic study of the 2011 January 3 Circleville earthquake, *Geophys. J. Int.* **189,** 1148–1158, doi: 10.1111/j.1365-246X.2012.05420.x.

Arrowsmith, S. J., J. B. Johnson, D. P. Drob, and M. A. H. Hedlin (2010). The seismo-acoustic wavefield: A new paradigm in studying geophysical phenomena, *Rev. Geophys.* **48,** RG4003, doi: 10.1029/2010RG000335.

Assink, J. D., G. Averbuch, P. S. M. Smets, and L. G. Evers (2016). On the infrasound detected from the 2013 and 2016 DPRK's underground nuclear tests, *Geophys. Res. Lett.* **43,** 3526–3533, doi: 10.1002/2016GL068497.

Assink, J. D., A. Le Pichon, E. Blanc, M. Kallel, and L. Khemiri (2014). Evaluation of wind and temperature profiles from ECMWF analysis on two hemispheres using volcanic infrasound, *J. Geophys. Res. Atmos.* **119,** 8659–8683, doi: 10.1002/2014JD021632.

Brachet, N., D. Brown, R. Le Bras, P. Mialle, and J. Coyne (2010). Infrasound monitoring for atmospheric studies, in *Monitoring the Earth's Atmosphere with the Global IMS Infrasound Network*, Springer, Dordrecht, The Netherlands, 77–118, ISBN: 978-1-4020-9507-8.

Brown, D. J., C. N. Katz, R. Le Bras, M. P. Flanagan, J. Wang, and A. K. Gault (2002). Infrasonic signal detection and source location at the prototype data centre, *Pure Appl. Geophys.* **159,** 1081–1125.

Cansi, Y. (1995). An automatic seismic event processing for detection and location: The P.M.C.C. method, *Geophys. Res. Lett.* **22,** 1021–1024.

Chiarabba, C., A. Amato, M. Anselmi, P. Baccheschi, I. Bianchi, M. Cattaneo, G. Cecere, L. Chiaraluce, M. G. Ciaccio, P. De Gori, *et al.* (2009). The 2009 L'Aquila (central Italy) M_w 6.3 earthquake: Main shock and aftershocks, *Geophys. Res. Lett.* **36,** L18308, doi: 10.1029/2009GL039627.

Chiaraluce, L., R. Di Stefano, E. Tinti, L. Scognamiglio, M. Michele, E. Casarotti, M. Cattaneo, P. De Gori, C. Chiarabba, G. Monachesi, *et al.* (2017). The 2016 Central Italy seismic sequence: A first look at the mainshocks, aftershocks, and source models, *Seismol. Res. Lett.*, **88,** no. 3, 757–771, doi: 10.1785/0220160221.

Cirella, A., and A. Piatanesi (2016). Source complexity of the 2016 Amatrice earthquake from non-linear inversion of strong motion data: Preliminary results, *Zenodo* doi: 10.5281/zenodo.153821.

Donn, W. L., and E. S. Posmentier (1964). Ground-coupled air waves from the Great Alaskan earthquake, *J. Geophys. Res.* **69,** no. 24, 5357–5361, doi: 10.1029/JZ069i024p05357.

Douglas, A., and P. D. Marshall (1996). Seismic source size and yield for nuclear explosions, in *Monitoring a Comprehensive Test Ban Treaty., NATO ASI Series (Series E: Applied Sciences)*, E. S. Husebye and A. M. Dainty (Editors), Springer, Dordrecht, The Netherlands, 303.

Drob, D. P., J. M. Picone, and M. Garcés (2003). Global morphology of infrasound propagation, *J. Geophys. Res.* **108,** no. D21, 4680, doi: 10.1029/2002JD003307.

Evers, L. G., D. Brown, K. D. Heaney, J. D. Assink, P. S. M. Smets, and M. Snellen (2014). Evanescent wave coupling in a geophysical system: Airborne acoustic signals from the M_w 8.1 Macquarie Ridge earthquake, *Geophys. Res. Lett.* **41,** 1644–1650, doi: 10.1002/2013GL058801.

Garcés, M., R. Hansen, and K. Lindquist (1998). Traveltimes for infrasonic waves propagating in a stratified atmosphere, *Geophys. J. Int.* **135,** doi: 10.1046/j.1365-246X.1998.00618.x.

Gibbons, S. J., V. Asming, L. Eliasson, A. Fedorov, J. Fyen, J. Kero, E. Kozlovskaya, T. Kværna, L. Liszka, S. P Näsholm, *et al.* (2015). The European arctic: A laboratory for seismoacoustic studies, *Seismol. Res. Lett.* **86,** 917–928, doi: 10.1785/0220140230.

Godin, O. A. (2008). Sound transmission through water–air interfaces: New insights into an old problem, *Contemp. Phys.* **49,** 105–123.

Green, D. N., and D. Bowers (2010). Estimating the detection capability of the International Monitoring System infrasound network, *J. Geophys. Res.* **115,** D18116, doi: 10.1029/2010JD014017.

Green, D. N., J. Guilbert, A. Le Pichon, O. Sebe, and D. Bowers (2009). Modelling ground-to-air coupling for the shallow M_L 4.3 folkestone, United Kingdom, earthquake of 28 April 2007, *Bull. Seismol. Soc. Am.* **99,** no. 4, 2541–2551, doi: 10.1785/0120080236.

Green, D. N., J. Vergoz, R. Gibson, A. Le Pichon, and L. Ceranna (2011). Infrasound radiated by the Gerdec and Chelopechene explosions: Propagation along unexpected paths, *Geophys. J. Int.* doi: 10.1111/j.1365-246X.2011.04975.x.

Hernandez, B., M. Cocco, F. Cotton, S. Stramondo, O. Scotti, F. Courboulex, and M. Campillo (2004). Rupture history of the 1997 Umbria-Marche (central Italy) main shocks from the inversion of GPS, DInSAR and near field strong motion data. *Ann. Geophys.* **47,** no. 4, 1355–1376, doi: 10.4401/ag-3349.

Lalande, J. M., O. Sèbe, M. Landès, Ph. Blanc-Benon, R. S. Matoza, A. Le Pichon, and E. Blanc (2012). Infrasound data inversion for atmospheric sounding, *Geophys. J. Int.* **190,** doi: 10.1111/j.1365-246X.2012.05518.x.

Lanzano, G., L. Luzi, F. Pacor, R. Puglia, M. D'Amico, C. Felicetta, and E. Russo (2016). Preliminary analysis of the accelerometric recordings of the August 24th, 2016 M_w 6.0 Amatrice earthquake, *Ann. Geophys.* **59,** doi: 10.4401/ag-7201.

Le Pichon, A., J. D. Assink, P. Heinrich, E. Blanc, A. Charlton-Perez, C. F. Lee, P. Keckhut, A. Hauchecorne, R. Rüfenacht, N. Kämpfer, *et al.* (2015). Comparison of co-located independent ground-based middle-atmospheric wind and temperature measurements with Numerical Weather Prediction models, *J. Geophys. Res. Atmos.* **120,** doi: 10.1002/2015JD023273.

Le Pichon, A., L. Ceranna, and J. Vergoz (2012). Incorporating numerical modeling into estimates of the detection capability of the IMS infrasound network, *J. Geophys. Res.* **117,** D05121, doi: 10.1029/2011JD016670.

Le Pichon, A., J. Guilbert, M. Vallée, J. X. Dessa, and M. Ulziibat (2003). Infrasonic imaging of the Kunlun Mountains during the great 2001 China earthquake, *Geophys. Res. Lett.* **30,** no. 15, doi: 10.1029/2003GL017581.

Le Pichon, A., P. Mialle, J. Guilbert, and J. Vergoz (2006). Multi-station infrasonic observations of the Chilean earthquake of 2005 June 13, *Geophys. J. Int.* **167,** no. 2, 838–844, doi: 10.1111/j.1365-246x.2006.03190.x.

Luzi, L., F. Pacor, and R. Puglia (2017). *Italian Accelerometric Archive v 2.3*, Istituto Nazionale di Geofisica e Vulcanologia, Dipartimento della Protezione Civile Nazionale, doi: 10.13127/ITACA.2.3 (in Italian).

Luzi, L., R. Puglia, E. Russo, M. D'Amico, C. Felicetta, F. Pacor, G. Lanzano, U. Çeken, J. Clinton, G. Costa, *et al.* (2016). The engineering strong-motion data-base: A platform to access Pan-European accelerometric data, *Seismol. Res. Lett.* **87,** doi: 10.1785/0220150278.

Madshus, C., F. Løvholt, A. Kaynia, L.R. Hole, K. Attenborough, and S. Taherzadeh (2005). Air-ground interaction in long range propagation of low frequency sound and vibration-field tests and model verification, *Appl. Acoust.* **66,** 553–578.

Marchetti, E., G. Lacanna, A. Le Pichon, D. Piccinini, and M. Ripepe (2016). Evidence of large infrasonic radiation induced by earthquake interaction with alluvial sediments, *Seismol. Res. Lett.* **87,** no. 3, 678–684, doi: 10.1785/0220150223.

Marty, J. (2018). The IMS infrasound network: Status and state-of-the-art design, in *Infrasound Monitoring for Atmospheric Studies, Challenges in Middle Atmospheric Dynamics and Societal Benefits*, Springer Nature, Dordrecht, The Netherlands, ISBN: 978-3-319-75140-5 (in press).

Matoza, R., M. Landès, A. Le Pichon, L. Ceranna, and D. Brown (2013). Coherent ambient infrasound recorded by the International Monitoring System, *Geophys. Res. Lett.* **40,** doi: 10.1029/2012GL054329.

Mialle, P., D. Brown, and N. Arora (2018). Advances in operational processing at the International Data Center, in *Infrasound Monitoring for Atmospheric Studies, Challenges in Middle Atmospheric Dynamics and Societal Benefits*, Springer Nature, Dordrecht, The Netherlands, ISBN: 978-3-319-75140-5 (in press).

Michele, M., R. Di Stefano, L. Chiaraluce, M. Cattaneo, P. De Gori, G. Monachesi, D. Latorre, S. Morzorati, L. Valoroso, C. Ladina, *et al.* (2016). The Amatrice 2016 seismic sequence: A preliminary look at the mainshock and aftershocks distribution, *Ann. Geophys.* **59,** doi: 10.4401/ag-7227.

Mikumo, T. (1968). Atmospheric pressure waves and tectonic deformation associated with the Alaskan earthquake of March 28, 1964, *J. Geophys. Res.* **73,** 2009–2025.

Mutschlecner, J. P., and R. W. Whitaker (2005). Infrasound from earthquakes, *J. Geophys. Res.* **110,** D01108, doi: 10.1029/2004JD005067.

Olson, J. V., C. R. Wilson, and R. A. Hansen (2003). Infrasound associated with the 2002 Denali fault earthquake, Alaska, *Geophys. Res. Lett.* **30,** no. 23, 2195, doi: 10.1029/2003GL018568.

Piccinini, D., N. A. Pino, and G. Saccorotti (2012). Source complexity of the May 20, 2012, M_w 5.9, Ferrara (Italy) event, *Ann. Geophys.* **55,** no. 4, doi: 10.4401/ag-6111.

Pisconti, A., E. Del Pezzo, F. Bianco, and S. de Lorenzo (2015). Seismic Q estimates in Umbria Marche (Central Italy): Hints for the retrieval of a new attenuation law for seismic risk, *Geophys. J. Int.* **201,** doi: 10.1093/gji/ggv055.

Ponceau, D., and L. Bosca (2010). Low-noise broadband microbarometers, in *Infrasound Monitoring for Atmospheric Studies*, Springer, Dordrecht, The Netherlands, 119–140, ISBN: 978-1-4020-9507-8.

Réseau Sismologique et géodésique Français (RESIF) (1995). RESIF-RLBP French broad-band network, *RESIF-RAP Strong Motion Network and Other Seismic Stations in Metropolitan France*, RESIF - Réseau Sismologique et géodésique Français, doi: 10.15778/resif.fr.

Shani-Kadmiel, S., J. D. Assink, P. S. M. Smets, and L. G. Evers (2018). Seismoacoustic coupled signals from earthquakes in central Italy: Epicentral and secondary sources of infrasound, *Geophys. Res. Lett.* **45,** doi: 10.1002/2017GL076125.

Snieder, R. (1986). The influence of topography on the propagation and scattering of surface waves, *Phys. Earth Planet. In.* **44,** no. 3, 226–241.

Szuberla, C. A. L., and J. V. Olson (2004). Uncertainties associated with parameter estimation in atmospheric infrasound arrays, *J. Acoust. Soc. Am.* **115,** 253–258, doi: 10.1121/1.1635407.

Terrana, S., J. P. Vilotte, and L. Guillot (2017). A spectral hybridizable discontinuous Galerkin method for elastic–acoustic wave propagation, *Geophys. J. Int.* **213,** no. 1, 574–602, doi: 10.1093/gji/ggx557.

Tinti, E., L. Scognamiglio, A. Michelini, and M. Cocco (2016). Slip heterogeneity and directivity of the M_L 6.0, 2016, Amatrice earthquake estimated with rapid finite-fault inversion, *Geophys. Res. Lett.* **43,** doi: 10.1002/2016GL071263.

Virieux, J., V. Etienne, and V. Cruz-Atienza (2012). Modelling seismic wave propagation for geophysical imaging, in *Seismic Waves– Research and Analysis*, Chapter 13, M. Kanao (Editor), 253–304, In-Tech, doi: 10.5772/1400.

Virieux, J., N. Garnier, E. Blanc, and J.-X. Dessa (2004). Paraxial ray tracing for atmospheric wave propagation, *Geophys. Res. Lett.* **31,** L20106, doi: 10.1029/2004GL020514.

Walker, K. T., A. L. Pichon, T. S. Kim, C. de Groot-Hedlin, I.-Y. Che, and M. Garcés (2013). An analysis of ground shaking and transmission loss from infrasound generated by the 2011 Tohoku earthquake, *J. Geophys. Res. Atmos.* **118,** no. 23, 12,831–12,851, doi: 10.1002/2013JD020187.

Waxler, R., and J. Assink (2018). Propagation modeling through realistic atmosphere and benchmarking, in *Infrasound Monitoring for Atmospheric Studies, Challenges in Middle Atmospheric Dynamics and Societal Benefits*, Springer Nature, Dordrecht, The Netherlands, ISBN: 978-3-319-75140-5 (in press).

Bruno Hernandez
Alexis Le Pichon
Julien Vergoz
Pascal Herry
Rémy Bossu[1]
CEA, DAM, DIF
F-91297 Arpajon
France

Lars Ceranna
Christoph Pilger
BGR
Stilleweg 2
D-30655 Hannover
Germany

Emanuele Marchetti
Maurizio Ripepe
Department of Earth Sciences
University of Firenze
Via G. La Pira, 4
50121 Florence
Italy

Published Online 5 September 2018

[1] Also at Euro-Mediterranean Seismological Centre, c/o CEA, DAM, DIF, F-91297 Arpajon, France.